Environmental Science Nano

PAPER

View Article Online
View Journal | View Issue

Cite this: *Environ. Sci.: Nano*, 2016, 3, 442

Received 16th September 2015,
Accepted 13th January 2016

DOI: 10.1039/c5en00201j

rsc.li/es-nano

Evaluation of toxicity of nanoclays and graphene oxide *in vivo*: a *Paramecium caudatum* study

Marina Kryuchkova,[a] Anna Danilushkina,[a] Yuri Lvov[ab] and Rawil Fakhrullin*[a]

We report here the successful use of a protozoan model organism *P. caudatum* to investigate the toxicity of clay nanoparticles (montmorillonite, halloysite, kaolin, and bentonite), silica nanospheres and graphene oxide nanoflakes. The distribution of nanoparticles inside the cells was investigated using enhanced dark-field microscopy. Biochemical and behavioural tests were employed to study the viability, vitality, nutrition and oxidative stress induction in ciliate protozoans. The nanoclay particles studied here exhibited very low or no toxicity towards *P. caudatum*, whereas graphene oxide was toxic.

Nano impact

Clay nanoparticles are arguably among the most industrially popular nanosized materials available in thousands of tons and extensively used in a number of applications. Consequently, the evaluation of toxicity of clay nanoparticles towards freshwater organisms is crucially important. This paper evaluates the toxic effects of several commercially available clay nanomaterials (montmorillonite, halloysite, kaolin, and bentonite) along with silica nanospheres and graphene oxide nanoparticles using a freshwater protozoan *Paramecium caudatum* as an *in vivo* model. Clay nanoparticles exhibit little or no toxicity, whereas graphene oxide exhibited profound toxicity.

Introduction

In recent years, the industrial and biomedical applications of nanosized clay particles have been rapidly increasing. Naturally occurring nanoclays, such as bentonite,[1] montmorillonite,[2] kaolin[3] and halloysite,[4] have been employed in a number of industrial applications, as nanosized fillers and as dopants to fabricate polymer composites and anticorrosion and flame-retardant protective coatings.[5,6] Nanoclay–polymer composites have found important biomedical applications, such as antimicrobial coatings,[7] nanocontainers for drug delivery,[8,9] bone healing implants,[10] paper-mimicking sheets,[11,12] pesticide carriers,[13] paint inclusion particles[14] and cosmetic formulations.[15] Nanoclay dopants considerably improve the macroscopic mechanical properties of polymer composites.[16,17] The impressive impact of nanoclay particles for the improvement of structural[18] and functional properties of (bio)materials together with their availability and low-cost production suggests that the use of nanoclay will be increasing continuously.[19]

The massive use of clay nanoparticles as polymer dopants suggests that they may be released during the material decomposition and are likely to pollute the natural habitats.[20] Montmorillonite, bentonite and kaolin are used in millions of tons for producing bulk ceramics; however, the increasing fraction of this industrial consumption is based on the exfoliation of these minerals into clay nanoparticles of ~1 nm thickness and hundreds of nanometres in width.[21] A more rare clay, halloysite (rolled kaolin sheets), was earlier used in bulk porcelain production but has now found numerous applications as polymer fillers, nanoceramic sorbents, exhaust catalysts or dispersants.[22] These applications demand the dispersion of the bulk clay particles into single nanosized particles: nanotubes of ~50 nm diameter and 1000 nm length. One could see that technology development is changing industrial applications of traditional clay minerals by converting them into nanosized particles of different shapes and morphologies. Thus, originating as natural minerals, they are converted into nanomaterials; consequently, their toxicity should be carefully analysed. Considering two important parameters, composition and shape, here we compare the toxicity of nanoclays with those of silica nanospheres and graphene oxide (GO) nanoflakes. All these nanoparticles have some degree of structural and morphological similarity based on multilayer formation of metal and silica oxide sheets.

Freshwater organisms are primarily expected to encounter clay nanoparticles released from the materials contacting water or soil. This implies that the outmost attention must be paid to the investigation of toxicity of clay nanoparticles

[a] *Bionanotechnology Lab, Kazan Federal University, Kreml uramı 18, Kazan, Republic of Tatarstan, Russian Federation. E-mail: kazanbio@gmail.com*
[b] *Institute for Micromanufacturing, Louisiana Tech University, Hegrot ave. 911, Ruston, LA, USA*

towards aqueous organisms. Among many other species, *Paramecium caudatum* has long been regarded as a viable model to investigate acute and long-term toxicity[23] of various compounds, including nanomaterials. *P. caudatum* is a free-living relatively large (up to 300 μm) transparent motile freshwater organism abundant in natural habitats. The motility of *P. caudatum* is regulated by coordinated beating of thousands of minute cilia covering the whole cell surface.[24] The diet of *P. caudatum* consists of microbial species, including bacteria, yeast and microalgae taken up inside the cell *via* the liquid flow facilitated with the cilia. Consequently, nanosized particles can be easily delivered into the protists during feeding.[25] The interesting feature of these protists is that they are single-cell eukaryotic organisms, which makes them simple and cheap yet functional models for performing *in vivo* tests. Here we, for the first time, employed *P. caudatum* to systematically investigate the toxic effects induced by a range of nanoclay particles and graphene oxide nanoflakes. We subjected the ciliates to nanoparticles dispersed in growth media and studied the growth rate, reproduction, nutrition, biochemical effects and behavioural responses of cells.

Methods

Chemicals

Nanoclay particles (kaolin, montmorillonite, and bentonite), silica nanoparticles and graphene oxide aqueous solution were purchased from Sigma-Aldrich. Halloysite nanotubes were provided by Applied Minerals Inc. (USA). All other chemicals were purchased from Sigma-Aldrich unless noted otherwise.

Paramecium caudatum culture

P. caudatum protozoan cells were cultivated in aqueous straw infusion growth media supplemented with NaCl (1.0 g L^{-1}), KCl (0.1 g L^{-1}), $NaHCO_3$ (0.2 g L^{-1}), $MgSO_4$ (0.1 g L^{-1}), and $CaCl_2$ (0.1 g L^{-1}) at 22–24 °C in the dark. Protozoans were fed with *Saccharomyces cerevisiae* yeast added into growth media. *P. caudatum* cells were harvested by centrifugation (300 rpm, 10 min) at the logarithmic phase of growth and washed if necessary. For certain experiments and imaging, the ciliates were picked up manually, using a micropipette. A LOMO MSP-1 stereomicroscope was used for the routine observation of the protists.

Characterisation techniques

Aqueous hydrodynamic diameters and zeta-potential of nanoparticles were measured in water at 25 °C using a Malvern Zetasizer Nano ZS instrument and standard plastic cells. Bright field and fluorescence microscopy images were collected using a Carl Zeiss Axio Imager microscope equipped with an AxioCam HRC CCD camera. Optical microscopy images were processed using ZEN software (Carl Zeiss). Atomic force microscopy images of nanoparticles were obtained using a Dimension FastScan instrument (Bruker) operated with Bruker Nanoscope software in ScanAsyst™ mode in air using silicon-nitride ScanAsyst Air probes (nominal tip radius of 2 nm). Diluted dispersions of nanoparticles were dropped onto clean glass substrates and dried in air. The raw AFM images obtained were processed using NanoScope Analysis v.1.6. software (Bruker). Enhanced dark field (EDF) microscopy images were obtained using an Olympus BX51 upright microscope equipped with a CytoViva® enhanced dark-field condenser and a DAGE CCD camera. A CytoViva® Dual Mode Fluorescence system was used to obtain transmission fluorescence images. Dust-free Nexterion® glass slides and coverslips (Schott) were used for EDF microscopy imaging to minimise dust interference.

Nanoparticle toxicity investigation

The toxicity of nanoclays (kaolin, montmorillonite, bentonite, and halloysite) and silica nanoparticles was investigated by adding the nanoparticles into *P. caudatum* growth media at 0.625, 1.25, 2.5, 5, and 10 mg mL^{-1}. Graphene oxide toxicity was studied at 0.0625, 0.125, 0.25, 1.5, 2 and 4 mg mL^{-1}. The cells were exposed to nanoclays and GO for 10, 30, and 60 min and 3, 5, and 24 hours. All experiments were performed in triplicate, and the data were presented as mean ± standard deviation.

Behavioural test (chemotaxis assay)

The chemotaxis assay was performed as described elsewhere.[23] Briefly, two adjacent growth media drops (0.01 mL) were placed onto the microscopy glass slide and positioned under the stereomicroscope. The first drop contained the appropriate concentration of nanoclays and silica (10 mg mL^{-1}) or GO (1 mg mL^{-1}), while the second was the pure media. 10 protozoans were placed into the nanoparticle-doped media drop, and then the drops were connected with the media bridge, allowing the free propulsion of protozoans between the drops. The chemotaxis was monitored microscopically by counting the number of cells in each drop for 1 hour at 15 min intervals. The behavioural reaction was considered positive if the cells remained inside the nanoparticle-supplemented drop, whereas the negative chemotaxis was detected if the cells migrated actively into the pure media.

Acute toxicity of nanoclay particles and GO

The cells (n = 7–10) were collected manually from the stock culture (24 hour growth) and were inoculated into the wells of cell culture plates. Then 20 μL of nanoparticles were added. The protozoans were incubated at 22–24°C without access to food. Viable and non-viable cells were counted using a stereomicroscope, and those cells which were immobile and did not preserve the typical shape were considered as dead. Control experiments were performed using the pure growth media only. The survival rate (N, %) was calculated as follows:

$$N = N_2/N_1 \times 100$$

where N_2 is the average number of protozoans at the end and N_1 is the average number of protozoans at the start of the experiment.

Vitality of protozoans

The reproduction activity (vitality) was investigated by placing a single protozoan cell into cell culture plate wells (24-well plates were used) and by monitoring the progeny growth rate. The appropriate volumes of nanoparticles and growth media (including yeast food) were added into wells. The effects of nanoparticles on fertility were evaluated as the reduction of binary fission rate compared to control cells.

Phagocytosis investigation

We investigated the effects of nanoclay, silica and GO particles on the intensity of phagocytosis in *P. caudatum* cells by counting the number of food vacuoles in cells after feeding with the nanoparticles. Protozoans (50 cells) were collected manually and placed into culture wells supplemented with 10 mg mL^{-1} of clay nanoparticles or silica. GO was added at 0.5 and 0.25 mg mL^{-1}, because the higher concentration caused the immediate lysis of cells. The cells were incubated for 1 or 24 hours, and then 10–15 protozoans were isolated and stained for 15 min using 0.1% aqueous Congo red dye which targets predominantly food vacuoles.[26] After staining, the cells were fixated using 2.5% buffered glutaraldehyde and washed with water. The vacuole number was counted using microphotographs obtained using the upright optical microscope.

Macronucleus morphology

The cells were incubated for 24 h in growth media supplemented with 10 mg mL^{-1} of silica/clay nanoparticles or 1 mg mL^{-1} GO. The effects of nanoparticles on the macronucleus morphology were investigated by staining the nuclei DNA with DAPI dye (0.1 mg mL^{-1}). Then the cells were imaged in white light and epifluorescence modes (UV excitation, DAPI emission narrow pass filter). The bright field and fluorescence images were then overlaid, and the overall shape and the numerical dimensions of the macronucleus (length, width, and stretching index) were estimated from the images.[27]

Oxidative stress indicators

P. caudatum cells were incubated for 24 h in growth media supplemented with 10 mg mL^{-1} of silica/clay nanoparticles or 1 mg mL^{-1} GO. After incubation, the cells were harvested at 2.5×10^5 mL^{-1}, cell counting was performed using a haemocytometer, and then the cells were ultrasonically disintegrated in 50 mM Tris-HCl buffer (pH 7.5) and collected by centrifugation.

Malondialdehyde concentration. Malondialdehyde concentration in cells was determined as published elsewhere.[28] A mixture of 500 μL of homogenised cells and 2.5 mL of 10% aqueous trichloroacetic acid was boiled at 100 °C for 15 min, cooled in ice and then separated by centrifugation. 2 mL of supernatant was mixed with 1 mL of 0.8% thiobarbituric acid, heated for 15 min at 100 °C and cooled, and then 1 mL of butanol was added. Optical absorption at 532 nm was measured using a Perkin Elmer Lambda 35 spectrophotometer.

Catalase activity. Catalase activity in cells was measured as described elsewhere.[29] Briefly, 50 μL of homogenized samples (750 μL in 100 mM phosphate buffer, pH 7.5) were supplemented with 200 μL of H_2O_2 (500 mM) and incubated at 25 °C. Catalase activity was measured at 240 nm using a Perkin Elmer Lambda 35 spectrophotometer.

Results

We focused on the investigation of the potential toxic effects caused by nanoclay particles currently used in tons in several industrial applications. Bentonite, montmorillonite and kaolin are platy clay particles ranging from nanometres to micrometres, whereas halloysite nanotubes are hollow rod-like particles having a lumen diameter of ~20 nm and a tube length ranging from 300 nm to 2 μm. Spherical silica nanoparticles were also used as a material mimicking the outer silica layer of the clays. Graphene oxide nanosheets having the shape and size close to smectite clays were selected as a material with relatively high reported toxicity,[30] which was also confirmed in our study. The typical AFM images demonstrating the geometry and sizes of nanoparticles used in this study are given in Fig. 1.

The nanoparticles used were suspended in water and added to protozoan media at a range of concentrations. Prior to toxicity investigation, the hydrodynamic diameters and surface potential of nanoparticles were determined using dynamic light scattering (DLS) and electrophoretic mobility measurements in water (Table 1).

P. caudatum cells exhibit a typical ellipsoid shape if imaged in bright field (Fig. 2a). The cells are fairly transparent which allows for visualisation of the organelles. Here we employed the enhanced dark field microscopy to observe the uptake of the clay nanoparticles by the protozoans. Fig. 2b shows a typical dark-field image of aggregated halloysite nanotubes being ingested by a *P. caudatum* cell in media with no food microorganisms. After ingestion, clay nanoparticles are transferred into the food vacuoles which were visualised either by EDF microscopy or by fluorescence microscopy (in the latter case, the nanoparticles were first labelled with Rhodamine B dye). In most cases, we resorted to the use of EDF microscopy, as this enabled us to avoid any interference from the dye itself.

In a typical toxicity experiment, the nanoparticles were administered to *P. caudatum* cells as an additive to the normal diet (yeast) at different concentrations, which resulted in the effective uptake of nanoparticles *via* the normal ingestion. We investigated a range of concentrations (from 0 to 10 mg mL^{-1}) for clay nanoparticles (montmorillonite, bentonite, halloysite and kaolin) and silica, whereas graphene oxide was

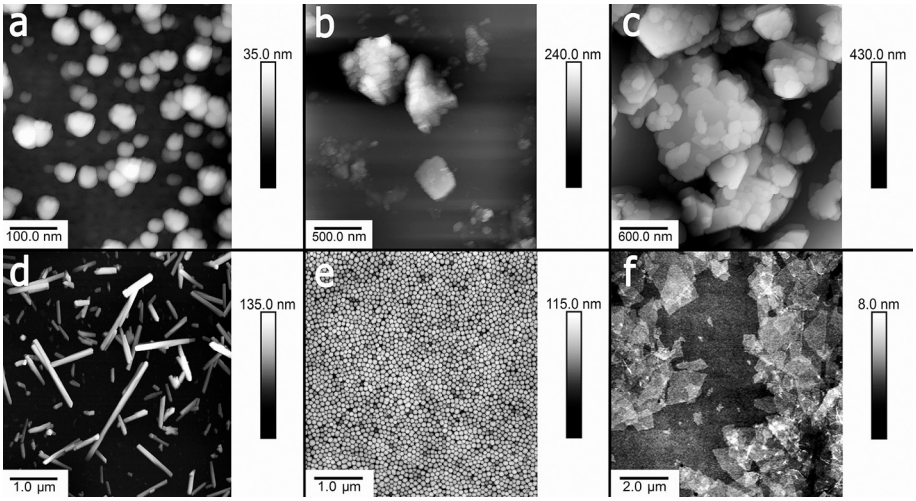

Fig. 1 Typical AFM images of a) bentonite, b) montmorillonite, c) kaolin, d) halloysite, e) silica and f) graphene oxide nanoparticles.

Table 1 Hydrodynamic diameters, zeta-potential values and AFM measured sizes of nanoclay particles, silica nanospheres and graphene oxide nanoflakes

Particles	Hydrodynamic diameter, nm	Zeta-potential, mV	AFM measured dimensions
Halloysite	510 ± 12	−25 ± 3	50 nm diameter, 400–1500 nm length
Kaolin	930 ± 22	−36 ± 1	300–700 nm width, 30–100 nm thick
Montmorillonite	1600 ± 60	−29 ± 1	300–600 nm width, 10–50 nm thick
Bentonite	3040 ± 660	44 ± 2	~4 μm width, ~100 nm thick
Silica	122 ± 3	−39 ± 6	120 nm diameter
Graphene oxide	1940 ± 90	−47 ± 2	2000 nm width, 2–10 nm thick

too toxic at high concentrations (2 mg mL^{-1}) leading to the immediate lysis of the cells upon contact; therefore, we have used lower concentrations of GO. We started with a simple behavioural test based on chemotaxis of protozoans offered two droplets of media, one of them containing nanoparticles at 10 mg mL^{-1} (Fig. 3a). The droplets were connected with a thin media bridge allowing for the free travelling of *P. caudatum* cells. The protozoans were inoculated into the nanoparticle-containing droplet, and their attraction or repulsion was observed under a microscope. Interestingly, the protozoans demonstrated the positive chemotaxis (~70%) towards halloysite, kaolin and montmorillonite, whereas the media droplets doped with silica and bentonite induced the overall negative chemotaxis (~80%) (Fig. 3b) at 10 mg mL^{-1}. Graphene oxide completely repulsed the protozoans at a much lower concentration (1 mg mL^{-1}) with no animals observed in the GO-doped droplets.

In the next set of experiments, we evaluated the acute toxicity of clay nanoparticles, silica colloid and graphene oxide nanosheets after the ingestion by the protozoans. The nanoparticles were admixed to the media containing yeast cells as the normal microbial diet. Typical EDF microscopy images of *P. caudatum* cells demonstrating the internalised nanoparticles are shown in Fig. 4.

The cells were then examined under a microscope to count the viable organisms and the dead cells. Dead cells were distinguished due to their diminished mobility, body deformation, visible cell lysis and membrane disruption. The results demonstrating the acute effects of nanoclay particles, silica nanospheres and graphene oxide nanoflakes on the viability of *P. caudatum* cells after 24 hours of co-incubation with yeast and nanoparticles are summarized in Fig. 5a, where the survival rates are shown. Overall, halloysite, kaolin and montmorillonite clay particles were not toxic at lower concentrations, even somewhat stimulating the growth of cells, which corresponds well with our previous studies.[31] Silica and bentonite appeared to be more toxic. The most profound reduction of survival rate was observed at higher concentrations (5 and 10 mg mL^{-1}), and graphene oxide was poisonous at 0.5 mg mL^{-1}.

We noticed that silica nanoparticles and bentonite also inhibited the asexual division (double fission) in *P. caudatum*, which was further investigated by employing a single cell progeny approach. To avoid any interference from *en mass* cultivation of cells, we isolated single cells and inoculated them into personal wells of plastic culture plates, and then the cell division was monitored constantly for 48 hours. The growth rate values obtained during the division of a single ancestor cell are shown in Fig. 5b.

Interestingly, clay nanoparticles did not inhibit the formation of food vacuoles in *P. caudatum* cells, while graphene oxide prevents their formation in cells. To investigate this important part of protozoan physiology, the cells were incubated with the nanoclay particles at the highest

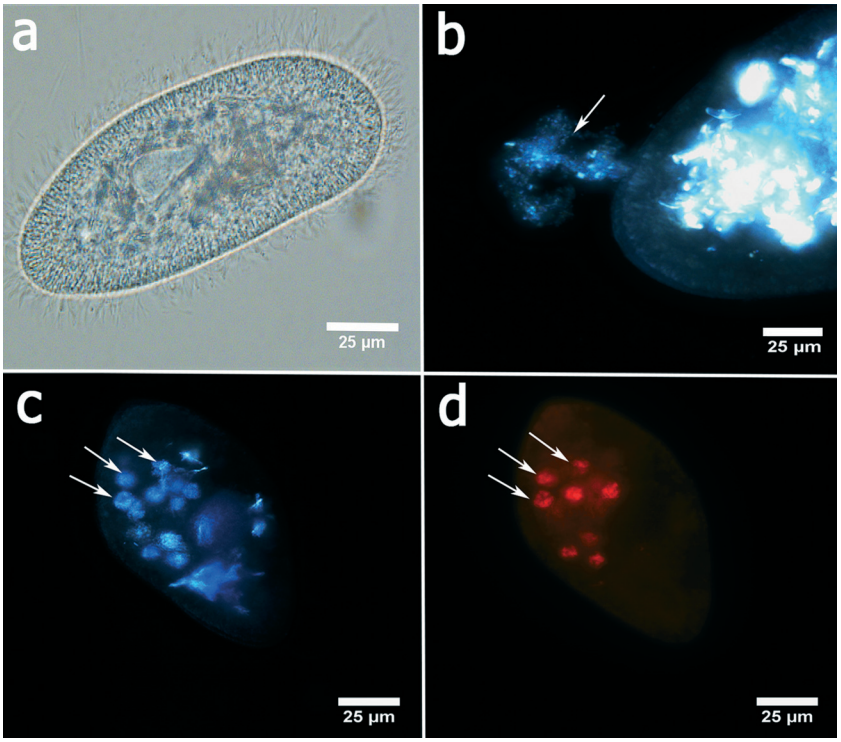

Fig. 2 Characterisation of *P. caudatum* morphology and nanoparticle ingestion: a) a typical optical microscopy image of *P. caudatum*; b) an EDF microscopy image demonstrating the ingestion of nanoclay particles (halloysite nanotubes) (indicated by an arrow) by *P. caudatum*; visualisation of nanoclay-filled food vacuoles (indicated by arrows) using c) EDF microscopy and d) fluorescence microscopy (nanoclay particles are stained with Rhodamine B prior to ingestion).

concentration (10 mg mL^{-1}), and then the cells were separated, fixated and stained with Congo red dye which selectively stains food vacuoles allowing for the effective counting using an upright microscope in bright field imaging mode. The typical optical microscopy images of food vacuoles in *P. caudatum* cells are given in Fig. 6.

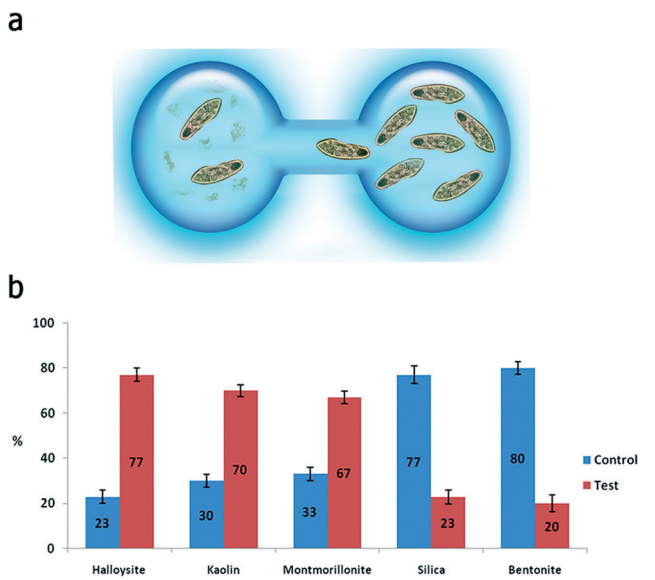

Fig. 3 Investigation of chemotaxis in *P. caudatum*: a) a sketch demonstrating the distribution of *P. caudatum* cells in droplets during the chemotaxis experiment; b) the distribution of *P. caudatum* cells in media and nanoparticle-doped droplets within 1 hour after inoculation.

Clay nanoparticles affect the food vacuole formation and, as a consequence, the digestion in *P. caudatum* protozoans. The short-term effects were observed after 1 hour of exposition, and the long-term effect was evaluated after 24 hours. The results are summarized in Fig. 7, where the data points are presented as percentage from the control (no nanoparticle exposure) values. Particularly, halloysite nanotubes exhibit the lowest reduction (12.2% and 27% for 1 hour incubation and 24 hour incubation, respectively), whereas bentonite and silica reduce the vacuole number in exposed cells almost twofold. These effects are prominent only at relatively high concentrations, whereas the lower concentrations studied did not induce any significant effects.

Another important morphological feature indicating the toxic influence on protozoans is the size and shape of the *P. caudatum* macronucleus which contains most of the DNA in *P. caudatum* cells. Here we employed a DNA-targeting fluorescence dye DAPI to stain macronuclei in clay nanoparticle-treated cells. Then the overlaid bright field and fluorescence images (Fig. 8) were used to evaluate the dimensions (length and width), total area and stretching index (the relation of macronuclei width to length).

The results are summarized in Table 2. Interestingly, no significant changes in the macronucleus morphology and

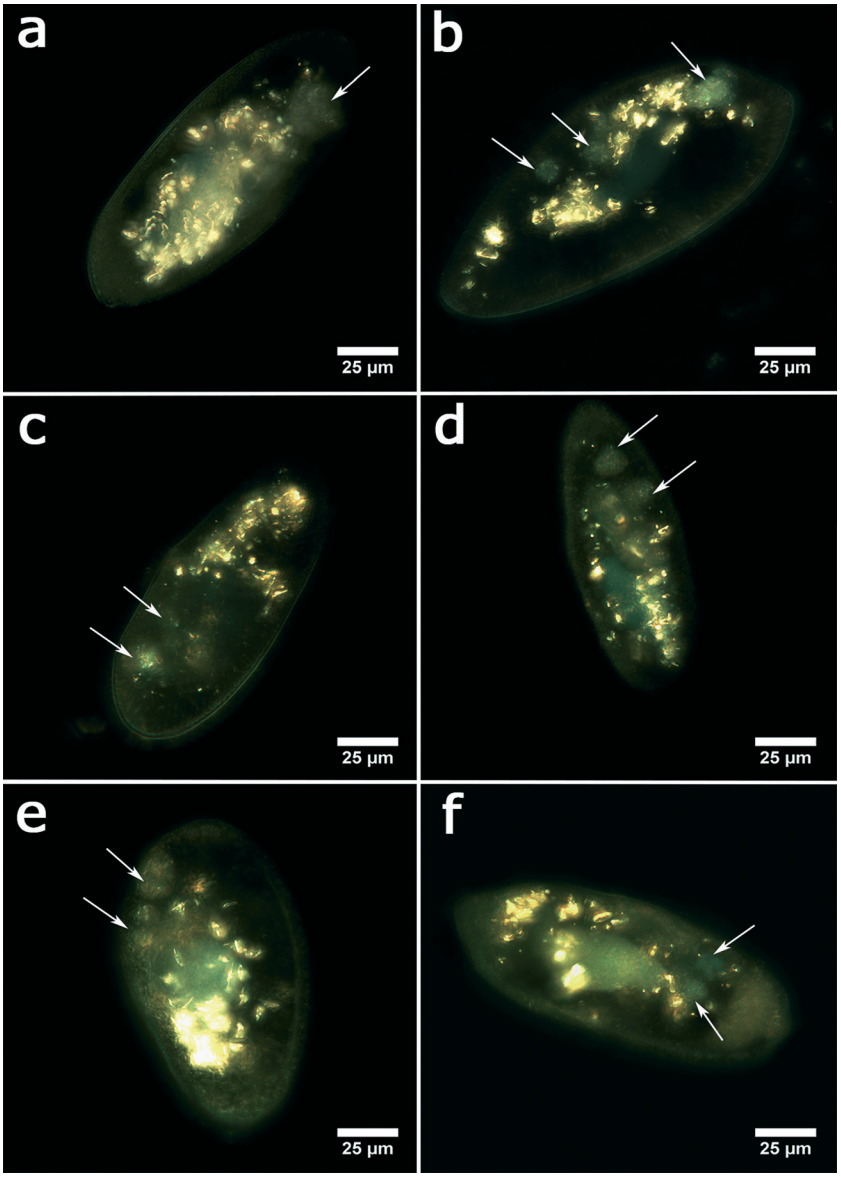

Fig. 4 Enhanced dark-field microscopy images of *P. caudatum*: a) intact cell and cells fed with b) halloysite, c) kaolin, d) montmorillonite, e) bentonite, and f) silica. Food vacuoles are indicated by arrows.

total area were observed in nanoclay-treated cells. We did not observed any morphological changes, such as rod shape deformity, vacuolization and diffusion, which are associated with genotoxic effects in *P. caudatum*.[27] However, graphene oxide nanosheets induced a significant increase in the total area of the macronucleus along with the occurrence of a rod shape deformity exhibiting the increased stretching index (Fig. 9d). These changes in the macronucleus morphology may indicate that the GO particles are concentrated in the macronucleus and potentially intercalate with DNA molecules of ciliates. This phenomenon requires additional attention and will be investigated in a follow-up study.

Graphene oxide was chosen here as a nanomaterial with previously reported toxicity.[32] Graphene oxide was severely toxic to *P. caudatum* cells. First, the cells demonstrated a strong negative chemotaxis towards GO at 1 mg mL^{-1}. Higher concentrations of graphene oxide, starting from 2 mg mL^{-1}, induced the sudden reduction of motility followed by the immediate cell lysis upon the contact. Therefore, we used the reduced concentrations of GO (0.0625 to 1.5 mg mL^{-1}) for the acute toxicity study (Fig. 9a). We determined the LD_{50} value of the GO concentration relevant to *P. caudatum*, which was 0.94 mg mL^{-1} (for 3 hour exposition) (Fig. 9b).

Graphene oxide inhibited phagocytosis in *P. caudatum* cells, and the exposed cells did not form food vacuoles within the whole range of concentrations studied. If administered at lower concentrations, GO nanoflakes were diffusely distributed in the cytoplasm, as confirmed by using EDF microscopy (Fig. 9c). It is likely that some fraction of GO nanoflakes might be attached to the cell surface as well; however, the

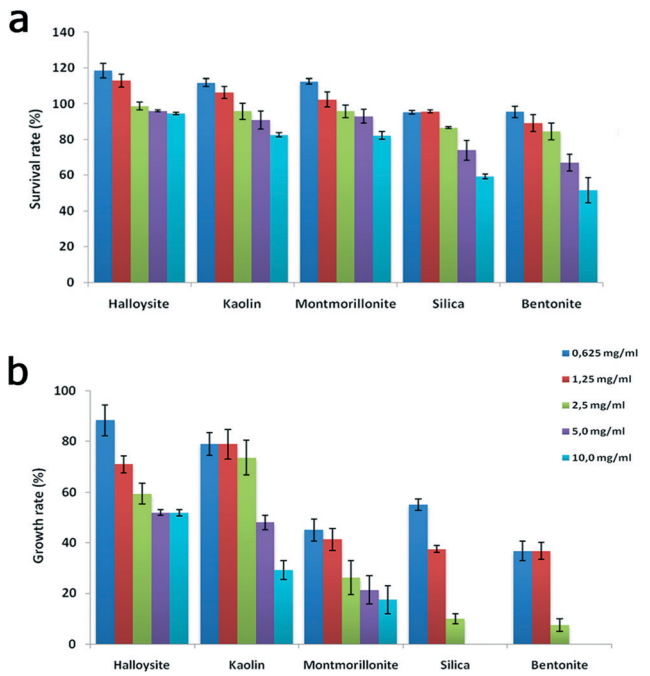

Fig. 5 Acute toxicity testing: a) survival rate and b) growth rate of *P. caudatum* cells exposed to increasing concentrations of nanoparticles.

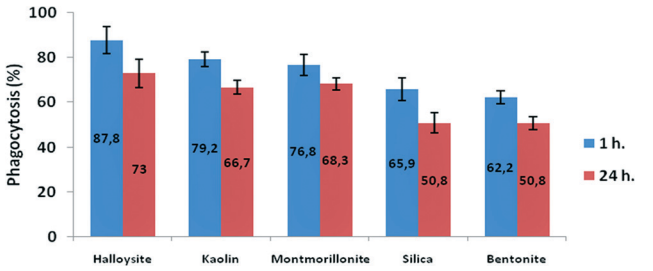

Fig. 7 The effects of clay nanoparticles on phagocytosis activity measured as the efficiency of food vacuole formation in *P. caudatum*.

direct EDF microscopy observation using a changing focal plane suggests that most of the GO particles are localised within the cytoplasm. Visually, this led to the darker appearance of the cells if observed in white light (not shown). The concentrations below 0.5 mg mL^{-1} did not affect the motility of the cells; however, starting with 1.5 mg mL^{-1} (which is higher than LD_{50}), the cellular motility was swiftly arrested upon introduction of GO. This effect might be mediated by the interaction of diffusely distributed GO nanosheets with contractile vacuoles in *P. caudatum* cells.

Finally, to evaluate the biochemical effects of nanoclay particles, we studied the oxidative stress induction in nanoparticle-treated cells monitored *via* malondialdehyde concentration measurements and antioxidant enzyme catalase activity. We found (Fig. 10) that clay nanoparticles (10 mg mL^{-1}) only slightly (3–6%) increased the malondialdehyde concentration in *P. caudatum* and negligibly increased the activity of catalase enzyme, whereas 1 mg mL^{-1} of GO implemented a more than 20% increase indicating the severe induction of oxidative stress. Malondialdehyde and catalase induction are the clear indicators of oxidative stress in *Paramecia*,[33] signifying the increased levels of hydrogen peroxide and superoxide radicals. Our results correspond well with the previous studies demonstrating the induction of oxidative stress by GO in human cells.[34] In addition, genotoxicity of carbon nanomaterials due to oxidative stress was also suggested.[35,36] Although additional studies are still required, our current results indicate that clay nanoparticles exhibit a very low toxicity level if compared with carbon nanomaterials (graphene oxide nanoflakes).

Discussion

P. caudatum protozoans are a powerful model organism to investigate the toxic effects of a wide range of substances, including colloid nanoparticles. Importantly, the simple behavioural patterns can also be monitored. The cells are relatively large (reaching 0.3 mm) as compared with bacteria, yeast and human cells routinely used in toxicity tests. The protozoans actively move due to the coordinated motion of the cilia covering their stiff cell membrane and feeding on

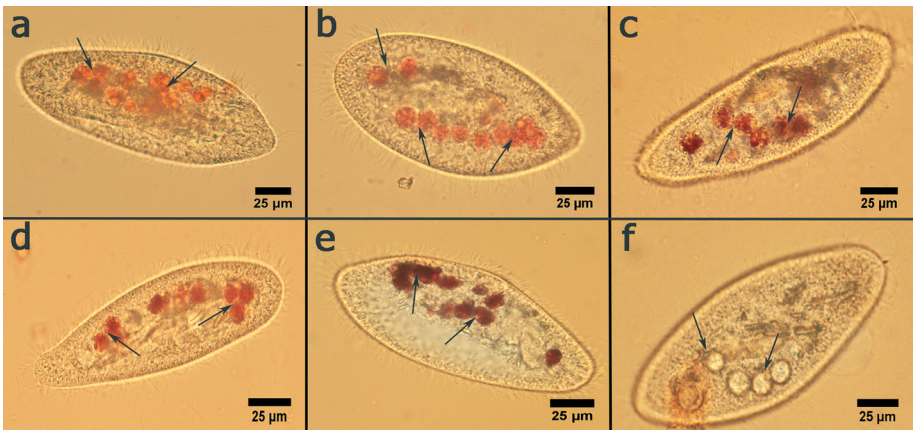

Fig. 6 Optical microscopy images of Congo red-stained food vacuoles in *P. caudatum*: a) intact cell and cells fed with b) halloysite, c) kaolin, d) montmorillonite, e) bentonite, and f) silica. Food vacuoles are indicated by arrows.

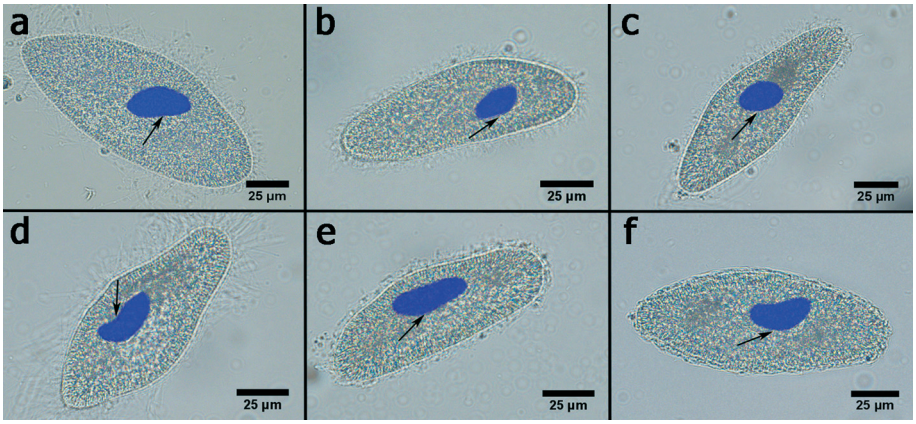

Fig. 8 Optical/fluorescence microscopy images of DAPI stained macronuclei in *P. caudatum*: a) intact cell and cells fed with b) halloysite, c) kaolin, d) montmorillonite, e) bentonite, and f) silica. Macronuclei are indicated by arrows.

microorganisms inhabiting the media. The clustered aggregates of nanomaterials used in our study were ingested *via* sweeping microorganisms into the oral groove and then into the mouth by the cilia. Light-scattering nanoparticles, including clay nanoparticles studied here, can be easily visualised inside the transparent bodies of *P. caudatum* using enhanced dark-field microscopy, in the same way as with *C. elegans* microworms.[37] It is likely that the potential of *P. caudatum* in toxicity testing of nanomaterials will be increased by introduction of novel behavioural tests similar to the ones recently described.

Our results indicate that *P. caudatum* cells are able to distinguish between the different types of clay nanoparticles and to avoid those ones which are more toxic towards them. We assume that the relatively larger negatively-charged particles (halloysite, kaolin and montmorillonite) might be mistakenly recognised as microbial food. *P. caudatum* cells, although being primitive unicellular organisms, are arguably able to be learned with several simple stimuli.[38] It is too preliminary to speculate if *P. caudatum* protists can be attracted by nanoclays as they are by several organic compounds;[23] however, the clear avoiding behaviour demonstrated in the case of GO nanoflakes suggests that the cells preferentially choose the nanoclay particles. All the nanoclay particles significantly affected the cell's vitality at higher concentrations (5 and 10 mg mL^{-1}), particularly silica nanoparticles and bentonite severely inhibited asexual division with no daughter cells observed in the samples during the whole assay. On the contrary, kaolin and specifically halloysite were not cytostatic at the lower concentrations, whereas at the higher concentrations they reduced the cell division almost twofold. We suppose that comparatively higher toxicity of silica nanoparticles might be caused by the smaller sizes (120 nm) facilitating their redistribution inside the cells. Bentonite samples employed in our study exhibit positive surface potential which may also contribute to the increased toxicity if compared with negatively charged particles (halloysite, kaolin, and montmorillonite). The effects of low cytostatic activity of halloysite nanotubes on dividing yeast and microscopic worms have been reported previously.[31,37]

Importantly, all GO concentrations studied here completely suppressed the reproduction in *P. caudatum*. The reasons behind this are still unclear; however, we hypothesize that both the interaction with DNA in the macronucleus and the inhibition of motility required for the successful binary fission might be responsible for the extreme inhibition of fertility in protozoans by graphene oxide. The mechanisms of the GO toxicity are still unclear, although the microbial cell membranes were demonstrated to repulse GO particles, thus suggesting intercellular toxicity induction *via* a biochemical pathway.[39] Currently, graphene-based materials are being actively developed worldwide,[40] which implies the increased attention towards its safety.[41] Particularly important was the fact that GO induced the substantial morphological changes in *P. caudatum* nuclei. It is known that GO effectively binds with cellular DNA and causes DNA damage in isolated human cells.[42] It is likely that the same effects may be implied by GO nanoflakes in ciliates, leading to severe consequences (cell death, mutations, *etc.*). On the other hand, we found that ciliates demonstrate higher tolerance to GO, if compared with bacteria[43] and mammal cell cultures,[44] which are typically more vulnerable to GO (sizable toxic effects start well below 100 μg mL^{-1}). In our study, we used GO nanoflakes merely as a positive control toxic substance to compare with nanoclays. However, after careful examination of the data obtained, we suggest that a more thorough investigation of

Table 2 Macronucleus dimensions in *Paramecium caudatum*

Exposure – 24 h	Length (NL), μm	Width (NW), μm	Nucleus size (NS), μm^2	Stretching index (NW/NL)
Untreated	34.3 ± 3.7	16.7 ± 2.4	899 ± 200	0.49 ± 0.05
Halloysite	30.1 ± 2.5	16.5 ± 2.3	780 ± 120	0.55 ± 0.10
Kaolin	31.1 ± 5.1	18.4 ± 2.5	897 ± 180	0.59 ± 0.10
Montmorillonite	34,8 ± 3.2	16.4 ± 2.3	896 ± 150	0.48 ± 0.08
Bentonite	33.5 ± 4.6	16.6 ± 3.2	880 ± 220	0.50 ± 0.06
Silica	33.2 ± 5.5	15.8 ± 2.3	822 ± 140	0.49 ± 0.11
Graphene oxide	42.2 ± 3.7	14.1 ± 1.1	938 ± 130	0.34 ± 0.03

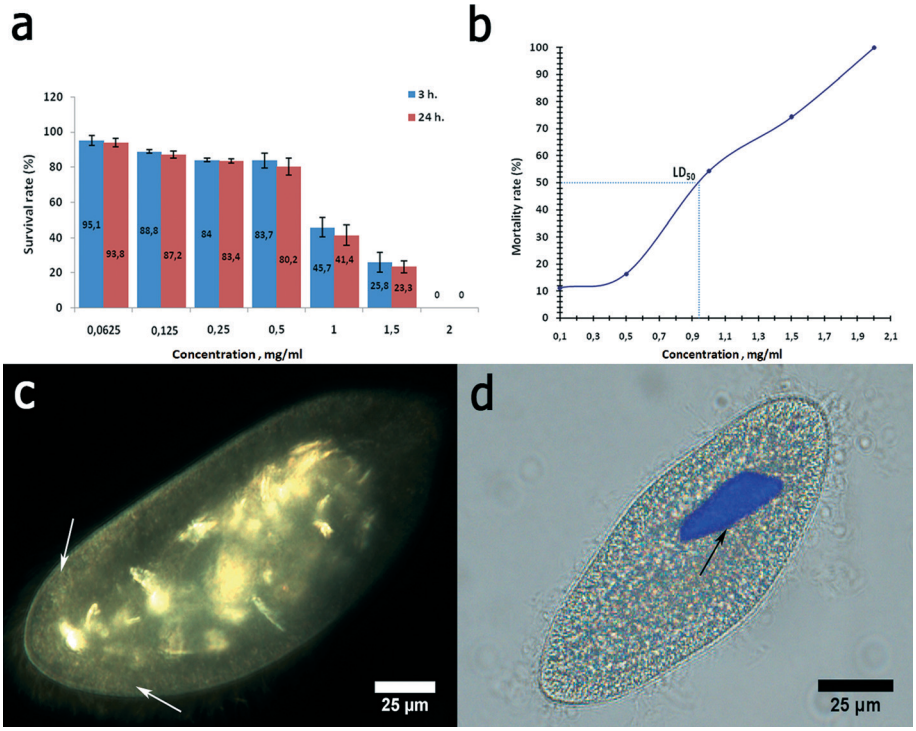

Fig. 9 Graphene oxide nanoflakes toxicity towards *P. caudatum* cells: a) survival rate; b) LD_{50} determination; c) EDF microscopy image demonstrating the distribution of GO nanoflakes in *P. caudatum*; d) *P. caudatum* macronucleus exhibiting the rod shape deformity after encountering GO nanoflakes.

the toxicity of graphene-based materials is required to avoid severe environmental problems after the potential exposure.

All the chosen nanoparticles, except graphene oxide, exhibit outer surfaces enriched with SiO_2, while GO has a surface enriched with CO groups and its shape and size are close to platy clays (montmorillonite and kaolin). Therefore, we assume that the higher toxicity of graphene oxide is more related to its surface chemistry rather than its shape. Besides, in millions of years of evolution, microorganisms, including protists, get used to coexisting with clay colloids which are present at large concentrations in river waters, while encountering colloid graphene oxide is extremely unusual for these live species. Considering a typical concentration of clay additives in polymeric composites of 5 wt%, 1 cm^3 of such composites contains 50 mg of clay nanoparticles. A slow release of this amount of nanoparticles gives hundred times dilution resulting in a safe nanoclay concentration, less than 0.5 mg mL^{-1}. In bio-decomposable polymeric composites, the release of clay nanoparticles is faster and the environment pollution rate may be higher.[4,11] Therefore, in landfills, one has to take care to prevent drainage of released nanoclays to the outside water reservoirs. A more dangerous situation may occur in the clay processing industry where powerful milling and high speed powder air centrifugation are used to produce tens of tons of nanoclays per day. It appears that the dangerous exposure to nanoclays may happen mostly not due to the decomposition of nanomaterials but rather due to malfunction in processing of clay minerals to nanosized powders. Clay minerals are generally believed to be safe,[45] although most of the studies performed so far were based on *in vitro* models utilizing human cell cultures[46] and a relatively low concentration range (up to 1 mg mL^{-1}) of nanoclays.[47] Here we employed a protozoan model subjected to a much higher concentration of nanoclay particles (up 10 mg mL^{-1}) to find out that such industrially relevant nanoclays[21] as halloysite,

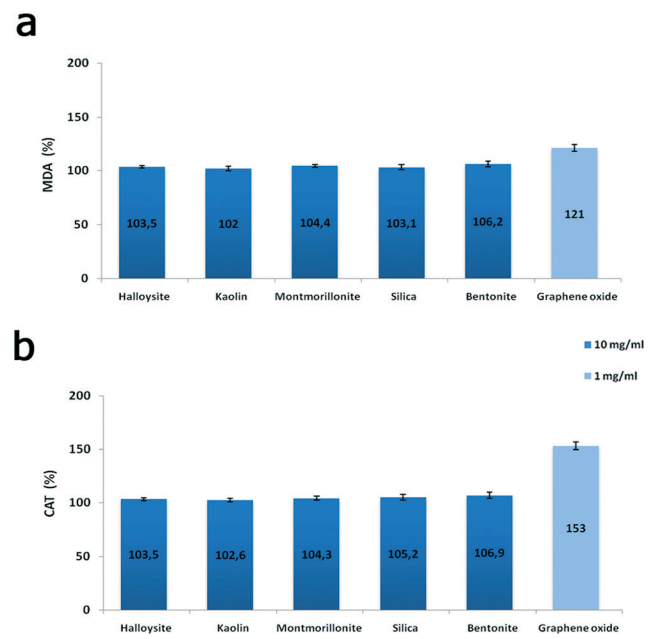

Fig. 10 Oxidative stress induction in *P. caudatum*: a) malondialdehyde concentration; b) catalase activity.

kaolin and montmorillonite are non-toxic towards freshwater ciliates. Our results indicate that nanoclay particles are relatively safe for scalable industrial use because they affect several important cellular functions in protozoans only at very high concentrations unlikely to be reached in real habitats.

Conclusion

The major result of our study clearly demonstrates that the toxicity of all nanoclays tested here is lower that of the similar size silica or graphene oxide particles. Among analysed nanoclays, halloysite nanotubes are the most biocompatible and hence may be safely used for different industrial applications, including biomedical ones. We compared the toxicity of nanoclays used in thousands of tons in modern industry with those of silica and graphene oxide, considering the shape, size and surface chemistry of these nanoparticles. We have chosen particles having approximately the same hydrodynamic diameters but of different shapes (platy, tubes and spheres) and with different surface compositions. The biosafety of the nanoparticles studied may be placed in the following order: the safest halloysite > kaolin > montmorillonite > silica > bentonite > graphene oxide. Up to 10 mg mL^{-1} of halloysite nanotubes were safe for one of the most common fresh water ciliate protist *P. caudatum*. This is 10 times more than the generally accepted safe halloysite dose for different cell cultures[47] (1 mg mL^{-1}) and indicates that there is an additional protection against nanoparticle effects on this microorganism survival.

Acknowledgements

This study was supported by Russian Science Foundation grant No. 14-14-00924. The authors thank Ms. A. Dubkova for technical help with microscopy images.

References

1 S. Pramanik, G. Das and N. Karak, *RSC Adv.*, 2013, **3**, 4574–4581.
2 C. A. Diaz, Y. Xia, M. Rubino, R. Auras, K. Jayaraman and J. Hotchkiss, *Nanoscale*, 2013, **5**, 164–168.
3 D. Boström, A. Grimm, C. Boman, E. Björnbom and M. Öhman, *Energy Fuels*, 2009, **23**, 5184–5190.
4 G. Cavallaro, G. Lazzara, S. Konnova, R. Fakhrullin and Y. Lvov, *Green Mater.*, 2014, **2**, 232–242.
5 Y. M. Lvov, D. G. Shchukin, H. Möhwald and R. R. Price, *ACS Nano*, 2008, **2**, 814–820.
6 B. Fang, L. Peng, Z. Xu and C. Gao, *ACS Nano*, 2015, **9**, 5214–5222.
7 W. Wei, R. T. Minullina, E. Abdullayev, R. F. Fakhrullin, D. Mills and Y. M. Lvov, *RSC Adv.*, 2014, **4**, 488–494.
8 V. Vergaro, E. Abdullayev, R. Cingolani, Y. Lvov and S. Leporatti, *Biomacromolecules*, 2010, **11**, 820.
9 M. R. Dzamukova, E. A. Naumenko, Y. M. Lvov and R. F. Fakhrullin, *Sci. Rep.*, 2015, **5**, 10560–10571.
10 G. Kapusetti, N. Misra, V. Singh, S. Srivastava, P. Roy, K. Danad and P. Maiti, *J. Mater. Chem. B*, 2014, **2**, 3984–3997.
11 G. Cavallaro, G. Lazzara, S. Milioto, F. Parisi and V. Sanzillo, *ACS Appl. Mater. Interfaces*, 2014, **6**, 606–612.
12 A. Liu and L. A. Berglund, *Eur. Polym. J.*, 2013, **49**, 940–949.
13 Y. Xiang, M. Wang, X. Sun, D. Cai and Z. Wu, *ACS Sustainable Chem. Eng.*, 2014, **2**, 918–924.
14 A. T. Saber, K. A. Jensen, N. R. Jacjbsen, R. Birkedal, L. Mikkelsen, P. Møller, S. Loft, H. Wallin and U. Vogel, *Nanotoxicology*, 2012, **6**, 453–471.
15 Y. J. Suh, D. S. Kil, K. S. Chung, E. Abdullayev, Y. M. Lvov and D. Mongayt, *J. Nanosci. Nanotechnol.*, 2011, **11**, 661–665.
16 B. Chen, J. Evans, H. C. Greenwell, P. Boulet, P. V. Coveney, A. A. Bowden and A. Whiting, *Chem. Soc. Rev.*, 2008, **37**, 568–594.
17 J. Carretero-Gonzalez, H. Retsos, E. P. Giannelis, T. A. Ezquerra, M. Hernandez and M. A. Lopez-Manchado, *Soft Matter*, 2009, **5**, 3481–3486.
18 B. Chen and J. R. G. Evans, *Soft Matter*, 2009, **5**, 3572–3584.
19 X. Lai, M. Agarwal, Y. Lvov, C. Pachpande, K. Varahramyan and F. Witzmann, *J. Appl. Toxicol.*, 2013, **33**, 1316.
20 S. Maisanaba, M. Puerto, S. Pichardo, M. Jorda, F. J. Moreno, S. Aucejo and A. Jos, *Food Chem. Toxicol.*, 2013, **57**, 266–275.
21 Y. M. Lvov, W. Wang, L. Zhang and R. F. Fakhrullin, *Adv. Mater.*, 2016, DOI: 10.1002/adma.201502341.
22 N. M. Sanchez-Ballester, G. V. Ramesh, T. Tanabe, E. Koudelkova, J. Liu, L. K. Shrestha, Y. Lvov, J. P. Hill, K. Ariga and H. Abe, *J. Mater. Chem. A*, 2015, **3**, 6614–6619.
23 N. Takiguchi, T. Tajima, K. Asayame, T. Ikeda, A. Kuroda, J. Kato and H. Ohtake, *J. Biosci. Bioeng.*, 2002, **93**, 416–420.
24 A. Funfak, C. Fisch, H. T. Abdel Motaal, J. Diener, L. Combettes, C. N. Baroud and P. Dupuis-Williams, *Integr. Biol.*, 2015, **7**, 90–100.
25 V. Aruoja, S. Pokhrel, M. Sihtmäe, M. Mortimer, L. Mädler and A. Kahru, *Environ. Sci.: Nano*, 2015, **2**, 630–644.
26 J. R. Nilsson, *Acta Protozool.*, 2003, **42**, 19–29.
27 M. M. Hussain, N. R. Amanchi, V. R. Solanki and M. Bhagavathi, *Pestic. Biochem. Physiol.*, 2008, **2**, 66–70.
28 H. H. Draper and M. Hadley, *Methods Enzymol.*, 1990, **186**, 241–431.
29 A. Claiborne, Catalase activity, in *CRC handbook of methods for oxygen radical research*, ed. R. A. Greenwald, CRC Press, Boca Raton, Florida, USA, 1985, vol. 1, pp. 283–284.
30 X. Guo and N. Mei, *J. Food Drug Anal.*, 2014, **22**, 105–115.
31 S. A. Konnova, I. R. Sharipova, T. A. Demina, Y. N. Osin, D. R. Yarullina, O. N. Ilinskaya, Y. M. Lvov and R. F. Fakhrullin, *Chem. Commun.*, 2013, **49**, 4208–4210.
32 A. B. Seabra, A. J. Paula, R. Lima, O. L. Alves and N. Duran, *Chem. Res. Toxicol.*, 2014, **27**, 159–168.
33 P. H. Hörtnagl and R. Sommaruga, *Photochem. Photobiol. Sci.*, 2007, **6**, 842–847.
34 Y. Chang, S.-T. Yanga, J.-H. Liua, E. Donga, Y. Wanga, A. Caoa, Y. Liua and H. Wang, *Toxicol. Lett.*, 2010, **200**, 201–210.
35 T. Kato, Y. Totsuka, K. Ishino, Y. Matsumoto, Y. Tada, D. Nakae, S. Goto, S. Masuda, S. Ogo, M. Kawanishi, T. Yagi, T. Matsuda, M. Watanabe and K. Wakabayashi, *Nanotoxicology*, 2012, **6**, 453–471.

36 A. Ivask, N. H. Voelcker, S. A. Seabrook, M. Hor, J. K. Kirby, M. Fenech, T. P. Davis and P. C. Ke, *Chem. Res. Toxicol.*, 2015, **28**, 1023–1035.
37 G. I. Fakhrullina, F. S. Akhatova, Y. M. Lvov and R. F. Fakhrullin, *Environ. Sci.: Nano*, 2015, **2**, 54–59.
38 H. L. Armus, A. R. Montgomery and J. L. Jellison, *Psychol. Rec.*, 2006, **56**, 489–498.
39 S. R.-V. Castrillón, F. Perreault, A. F. Faria and M. Elimelech, *Environ. Sci. Technol. Lett.*, 2015, **2**, 112–117.
40 A. Pourjavadi, M. Nazari and S. H. Hosseini, *RSC Adv.*, 2015, **5**, 32263–32271.
41 S. A. Sydlik, S. Jhunjhunwala, M. J. Webber, D. G. Anderson and R. Langer, *ACS Nano*, 2015, **9**, 3866–3874.
42 Y. Qiao, J. An and L. Ma, *Anal. Chem.*, 2013, **85**, 4107–4112.
43 Y. Tu, M. Lv, P. Xiu, T. Huynh, M. Zhang, M. Castell, Z. Liu, Q. Huang, C. Fan, H. Fang and R. Zhou, *Nat. Nanotechnol.*, 2013, **8**, 594–601.
44 Y. Li, Q. Wu, Y. Zhao, Y. Bai, P. Chen, T. Xia and D. Wang, *ACS Nano*, 2014, **8**, 2100–2110.
45 A. López-Galindo, C. Viseras and P. Cerezo, *Appl. Clay Sci.*, 2007, **36**, 51–63.
46 S. Maisanaba, S. Pichardo, M. Puerto, D. Gutiérrez-Praena, A. M. Cameán and A. Jos, *Environ. Res.*, 2015, **138**, 233–254.
47 F. R. Ahmed, M. H. Shoaib, M. Azhar, S. H. Umd, R. I. Yousuf, S. Hashmi and A. Dar, *Colloids Surf., B*, 2015, **135**, 50–55.

